Defect modeling in spreading nematic droplets

T.-S. Lin, L. Kondic, and L. J. Cummings
Department of Mathematical Sciences and Center for Applied Mathematics and Statistics, New Jersey Institute of Technology, Newark, New Jersey 07102, USA
(Received 3 May 2011; revised manuscript received 16 August 2011; published 13 January 2012)

Experiments by Poulard and Cazabat [Langmuir **21**, 6270 (2005)] on spreading droplets of nematic liquid crystal (NLC) reveal a surprisingly rich variety of behavior, including at least two different emerging length scales resulting from a contact line instability. In earlier work [Cummings, Lin, and Kondic, Phys. Fluids **23**, 043102 (2011)] we modified a lubrication model for NLCs due to Ben Amar and Cummings [Phys. Fluids **13**, 1160 (2001)] and showed that, in a qualitative sense, it can account for two-dimensional (2D) versions of the observed behavior. In the present work we propose a different approach that allows us to explore the effect of anchoring variations on the substrate, again in a 2D geometry. This in turn gives a simple way to model the presence of defects, which are nearly always present in such flows. The present model leads to additional terms in the governing equation. We explore the influence of these additional terms for some simple flow scenarios to gain insight into their influence.

DOI: 10.1103/PhysRevE.85.012702 PACS number(s): 83.80.Xz, 47.57.Lj, 47.15.gm, 47.20.Ma

The coating of a thin film of nematic liquid crystal (NLC) onto a substrate is one stage in the manufacture of liquid crystal display devices. For example, a recent experimental study [1] on coating and falling flows in the nematic phase was motivated by the search for improved manufacturing techniques for NLC microdisplay components. We refer readers to Ref. [2], which discusses many intriguing features of liquid crystals, and to Refs. [3,4] for more in-depth reviews of liquid crystal phenomenology. Coating may be unstable: When NLC droplets spread on silicon substrates, the contact line and the free surface are unstable at high relative humidity (greater than 60%) [5]. The observed behavior is complex: Depending on the exact conditions, droplets may either spread stably, spread unstably, or be arrested in their spreading (with or without destabilizing). Defects (discontinuities of the director field) appear to always accompany instabilities, but at this stage their role in the instability development is unclear: Whether defects induce the instabilities, are induced by them, or some other explanation altogether, is still an open question. In previous work [6] we presented a model and simulations supporting the idea that the elastic force due to the difference between two different surface anchoring conditions might be the instability mechanism. In this Brief Report we extend the model to investigate the influence of defects. Our approach is to derive a smoothed model of a defect in the continuum model, in which the director field varies continuously, but abruptly, in the region of the supposed defect. For clarity of exposition and maximum analytical progress we restrict attention here to a two-dimensional (2D) model in which the flow and director field are restricted to the (x,z) plane.

The main dependent variables governing NLC dynamics in this simple 2D case are the velocity field $\boldsymbol{v} = (u,0,w)$ and director field $\boldsymbol{n} = (\sin\tilde{\theta},0,\cos\tilde{\theta})$, the unit vector describing the averaged orientation of the anisotropic axis in the NLC [7]. The evolution equation of the film is derived in the lubrication (thin-film) limit. On the time scale of the fluid flow the director instantaneously adjusts to the flow conditions and so is always in equilibrium for the droplet geometry at that time. Thus the director angle $\tilde{\theta}$ is determined by minimizing the elastic free energy within the NLC, for the current free surface geometry. The details of the derivation are presented elsewhere [6] (see also Refs. [8,9]); here we only describe how we extend that model to include defects. The evolution of the film height $h(x,t)$ is given by a single partial differential equation (PDE) with a dependence on the normalized director angle $\theta = 2\tilde{\theta}/\pi$:

$$\frac{\partial h}{\partial t} + \frac{\partial}{\partial x}[h^3(\mathcal{C}h_{xxx} - \mathcal{B}h_x) - \mathcal{N}h^3\theta_z\theta_{zx}] = 0, \qquad (1)$$

where $\mathcal{C} = \delta^3\gamma/\mu U$ is an inverse capillary number, $\mathcal{B} = \delta^3\rho g L^2/\mu U$ is a Bond number, and $\mathcal{N} = K\pi^2/4\mu U L$ is an inverse Ericksen number. In these dimensionless groups, $\delta = H/L \ll 1$ is the aspect ratio between a typical drop height H and the length scale of typical variations in the x direction (L), so that dimensional coordinates (x^*,z^*) are related to dimensionless (x,z) by $(x^*,z^*) = L(x,\delta z)$. In addition, γ is the surface tension coefficient, $\mu = \alpha_4/2$ is chosen as a representative viscosity scaling (α_4 is one of the Leslie viscosities of the NLC), U is the typical flow velocity in the plane of the substrate, ρ is the density, g is gravitational acceleration, and K is the elastic constant within the equal-elastic-constant approximation ($K_1 = K_3 = K$) [3].

The director field has a preferred orientation at different interfaces. Typical conditions are that at the free surface (NLC-air interface) the director tends to align normal to the interface (homeotropic anchoring), while at the flat substrate (NLC-solid interface) it tends to align parallel to the surface (planar anchoring). In Refs. [8,9], the cases of strong and uniform weak anchoring (respectively) are considered. We found [6] that the assumption of uniform weak anchoring was not satisfactory in the vicinity of a contact line (strong anchoring was less satisfactory still). In principle, for a relatively thick film the director can accommodate the two (different) preferred angles at the substrate and free surface almost exactly, but for a very thin film it cannot [10]. We introduced an *ad hoc* anchoring condition based on specifying the change in normalized director angle across the film [6],

$$\theta = \theta_0 + \frac{\Theta m(h)}{h} z. \qquad (2)$$

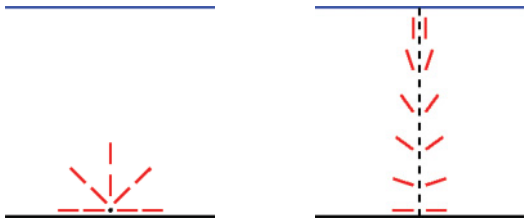

(a)Point defect, (b)line defect, in 2D drop.

FIG. 1. (Color online) Schematic of the two defect types considered. The solid (blue) top curve indicates the free surface of a droplet, the solid (black) bottom curve indicates the solid substrate, short (red) lines represent the director field orientation, and the black point-dashed line indicates the defect location.

Strong planar anchoring is imposed on $z = 0$ so $\theta_0 = \pm 1$. At the free surface $z = h$, $\theta = \theta_0 + \Theta m(h)$, where Θ is the difference between the preferred anchoring angles at the two interfaces in the bulk flow and $m(h)$ is a monotonically increasing function, approaching zero as $h \to 0$ and approaching 1 as $h \to \infty$. Note that such a regularization can mean that either the anchoring strength at the free surface goes to zero as $h \to 0$ or the anchoring angle at the free surface relaxes to that at the substrate as $h \to 0$. Here, as in Ref. [6], we set

$$m(h) = \frac{h^{3/2}}{\beta^{3/2} + h^{3/2}}, \tag{3}$$

where β is a dimensionless anchoring relaxation length. For a film of height $h \ll \beta$ anchoring is weak and for $h \gg \beta$ it is strong (as $\beta \to 0$ we recover the strong anchoring model of Ref. [8]). For this particular choice of $m(h)$ the nematic term in the governing equation reduces to the same form as the gravity term as $h \to 0$ [see Eq. (5) with Θ constant; for more details see Ref. [6]], leading to droplets that spread faster than the Newtonian equivalents.

Here we introduce a simple model for defects that assumes $\Theta = \Theta(x)$ has (smoothed) discontinuities at specific locations. Figure 1 shows two possible defect configurations in two dimensions: a point defect, where the director is discontinuous at a single point, and a line defect, where the discontinuity is along a line. Reverting to dimensional coordinates (x^*, z^*) momentarily, it is clear that, for an idealized 2D line defect along $x^* = 0$, the director angle $\tilde{\theta}$ is linear in z^* away from the actual discontinuity (the sign of the linear multiplier of z^* changes as we cross the discontinuity). An idealized 2D point defect at (0,0), in contrast, is described locally by $\tilde{\theta} \approx -\tan^{-1}(x^*/z^*)$ (recall that $\tilde{\theta}$ is the angle the director makes with the vertical and by convention is negative when $x^* > 0$). At fixed distance $x^* = X^*$ and for $z^* \ll |X^*|$, this is approximated by $\theta = 2\tilde{\theta}/\pi \approx \mp 1 + 2z^*/\pi X^*$. For films thinner than the defect outer core size [11], this linear approximation (where the sign of the linear multiplier again changes as the defect is crossed and X^* changes sign) is valid everywhere outside the core; therefore, for sufficiently thin films, 2D point and line defects are asymptotically equivalent. In the spirit of using a 2D model to qualitatively represent 3D reality, we suggest that these idealizations can give insight into the behavior of 3D line and point defects [12].

Since defects are often associated with substrate inhomogeneities we assume they are fixed and preexisting. To model the change of director orientation across a defect, we assume that the difference Θ between the preferred normalized anchoring angles at the two interfaces changes smoothly from -1 to $+1$ via the prescription

$$\Theta(x) = \tanh\left(\frac{x - x_0}{w}\right), \tag{4}$$

where x_0 is the position and w is the effective dimensionless width of the defect (corresponding to a dimensional defect core width wL [11]). To the left of the defect, where $x_0 - x \gg w$, the director turns through a normalized angle (-1) across the film, while to the right of the defect where $x - x_0 \gg w$ it turns through a normalized angle $(+1)$. In our simulations we choose $w = 0.1$; the above defect formulation will be valid within the lubrication approximation provided $\delta \ll w$. Multiple defects, which are often observed, can be modeled by replacing Eq. (4) by a superposition of hyperbolic tangents. Combining Eqs. (1) and (2) gives the governing PDE

$$\frac{\partial h}{\partial t} + \frac{\partial}{\partial x}[h^3(\mathcal{C}h_{xxx} - \mathcal{B}h_x) + \mathcal{N}\Theta^2(m^2 h_x - hmm_x) - \mathcal{N}\Theta\Theta_x m^2 h] = 0, \tag{5}$$

with $m(h)$ and $\Theta(x)$ given by Eqs. (3) and (4), respectively. Equations similar in structure to Eq. (5) have been used extensively to model problems relevant to thin-film dynamics [13]. Equation (5) contains the parameters $\mathcal{C}$, $\mathcal{B}$, $\mathcal{N}$, and β as well as the location and width of any defects. Since parameter space is prohibitively large to explore, as discussed in Ref. [6], we fix the capillary length as the characteristic length scale $L = \sqrt{\gamma/\rho g}$ (equivalent to $\mathcal{C} = \mathcal{B}$) and set $\mathcal{C} = \mathcal{B} = 1$, fixing the scale of the spreading speed. This choice is appropriate for typical material properties [6]. Based on additional estimates given in Ref. [6], we also set $\mathcal{N} = 50$ and investigate the effects of β and of defects.

We first summarize the classic linear stability analysis (LSA) of a flat-film solution $h = h_0$ of the defect-free model, $\Theta(x) = 1$, given in Ref. [6]. Expanding $h(x,t) = h_0 + \epsilon h_1(x,t) + \cdots (0 < \epsilon \ll 1)$, with $h_1 = h_{10}\exp(ikx - \omega t)$, we obtain the dispersion relation

$$\omega = -h_0^3 k^2\{k^2 + [1 - \mathcal{N}M(h_0,\beta)]\},$$
$$M(h_0,\beta) = \frac{h_0^{3/2} - \frac{\beta^{3/2}}{2}}{\left(h_0^{3/2} + \beta^{3/2}\right)^3}.$$

The film is unstable to perturbations with $0 < k < k_c = \sqrt{\mathcal{N}M(h_0,\beta) - 1}$ if $\mathcal{N}M(h_0,\beta) > 1$; the fastest-growing wave number is $k_m = \sqrt{[\mathcal{N}M(h_0,\beta) - 1]/2}$. Even though the LSA is valid only for a flat film, it is still a good indicator for spreading surface instabilities [6].

Figure 2 shows the stability diagram for $\mathcal{N} = 50$ in (β, h_0) space. Without defects, a flat film is less stable when the dimensionless anchoring relaxation length β is small: Smaller β means larger free surface anchoring strength and higher destabilizing elastic forces within the film. In particular, in the strong anchoring limit $\beta = 0$ thick films are stable while all thin films are unstable. Figures 3–6 show numerical simulations of spreading droplets (initially smoothed rectangles

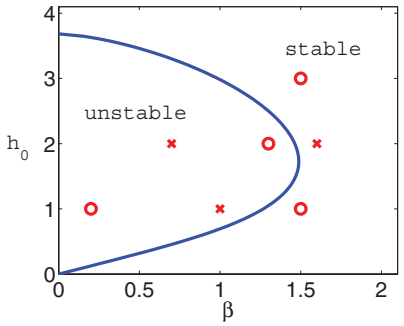

FIG. 2. (Color online) Stability diagram in (β, h_0) space for $\mathcal{N} = 50$. The region enclosed by the solid (blue) curve is unstable. (Red) Circles denote the parameters considered in Figs. 3–6. (Red) Crosses denote the parameters considered in Ref. [14].

of dimensionless height h_0 and width 10) with and without defects, for different choices of parameter values [marked by (red) circles in Fig. 2]. Additional simulations (marked by crosses) are presented as animations in Ref. [14]. In all cases solid curves show droplet profiles h, while dashed curves show the corresponding composite anchoring function $\Theta(x)\,m(h)$. In all cases, the moving contact line is regularized by a thin precursor film of thickness 0.01, as in Ref. [6].

Figure 3 shows a stable spreading scenario (with $\mathcal{N} = 50$, $\beta = 1.5$, and $h_0 = 3$). Figures 3(a) and 3(c) show the chosen initial condition (smoothed rectangle) and numerical results, respectively, at $t = 400$ without defects [$\Theta(x) \equiv 1$]; Figs. 3(b) and 3(d) show the corresponding results with three defects at $x_0 = -5$, 0, and 7. Consistent with LSA, there is no free

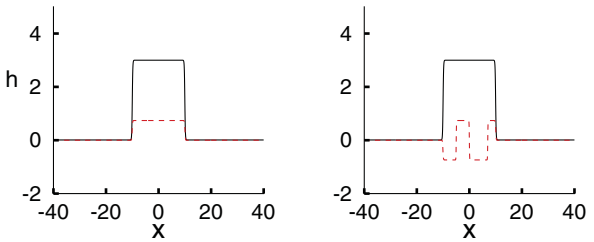

(a)$t = 0$, no defects. (b)$t = 0$, with defects at $x_0 = -5$, 0 and 7.

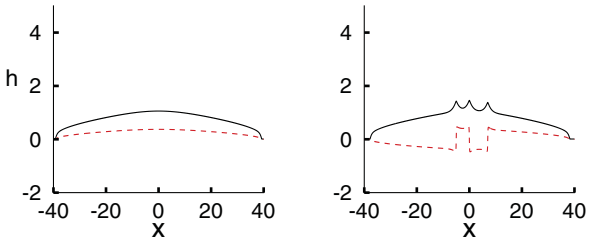

(c)$t = 400$, no defects. (d)$t = 400$, with defects at $x_0 = -5$, 0 and 7.

FIG. 3. (Color online) Simulations with $\mathcal{N} = 50$, $\beta = 1.5$, and $h_0 = 3$ from an initial smoothed rectangular profile with support $[-5,5]$ and height h_0. The solid (black) curves show the droplet profile h and the dashed (red) curves show the corresponding anchoring function $\Theta(x)\,m(h)$.

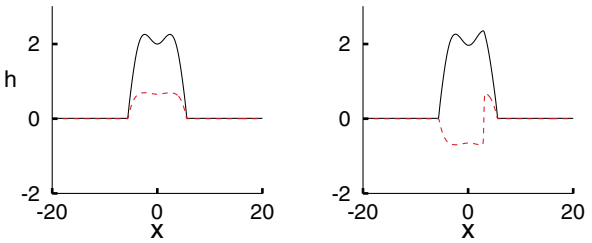

(a)$t = 0.1$, no defects. (b)$t = 0.1$, with a defect at $x_0 = 3$.

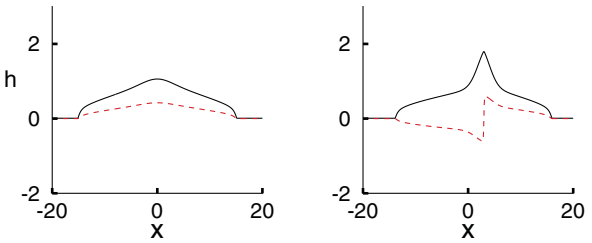

(c)$t = 100$, no defects. (d)$t = 100$, with a defect at $x_0 = 3$.

FIG. 4. (Color online) Simulations with $\mathcal{N} = 50$, $\beta = 1.3$, and $h_0 = 2$. Curve denotations and other details are the same as in Fig. 3.

surface instability; however, in Fig. 3(d) small crests appear at the defect locations [3]. These crests (the free surface gradient changes smoothly but abruptly over the length scale $w \gg \delta$) appear to be a robust feature of our simulations with defects. Note the change in anchoring function $\Theta(x)m(h)$ across a defect.

Figure 4 shows an unstable spreading scenario (with $\mathcal{N} = 50$, $\beta = 1.3$, and $h_0 = 2$). With no defects, in the early stages, the drop evolves from a rectangular profile into a drop with two humps [Fig. 4(a), solid line, $t = 0.1$]. As the drop spreads, these two humps merge and eventually disappear [Fig. 4(c), $t = 100$]. Figures 4(b) and 4(d) show the case with a defect at $x_0 = 3$. Symmetry is broken: One hump is pinned at the defect location and the hump on the left merges with this pinned hump, which persists.

Figure 5 shows an unstable nonspreading droplet [6] (with $\mathcal{N} = 50$, $\beta = 0.2$, and $h_0 = 1$). Even without defects [Fig. 5(a)], the initial profile breaks into five distinct humps,

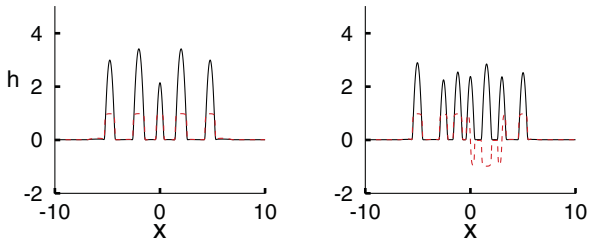

(a)$t = 5$, no defects. (b)$t = 5$, with defects at $x_0 = 0, 3$.

FIG. 5. (Color online) Simulations with $\mathcal{N} = 50$, $\beta = 0.2$, and $h_0 = 1$. Curve denotations are the same as in Fig. 3 and the initial conditions are shown by dash-dotted lines in (a).

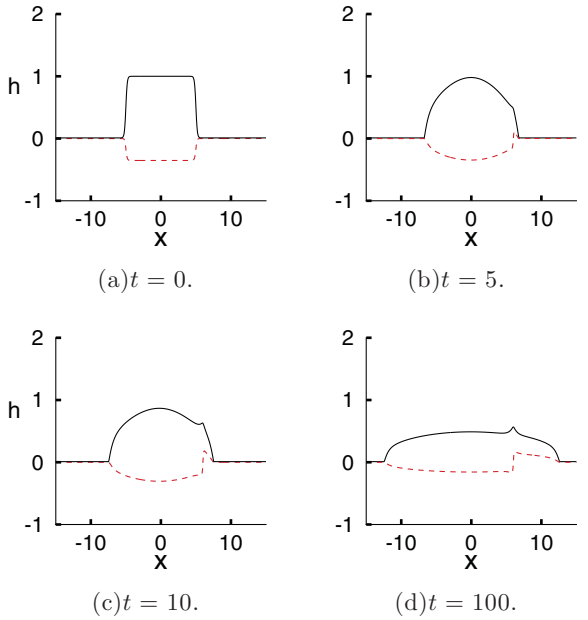

FIG. 6. (Color online) Simulations with $\mathcal{N} = 50$, $\beta = 1.5$, and $h_0 = 1$. A single defect is located at $x_0 = 6$, which is originally outside the droplet. Curve denotations are the same as in Fig. 3.

which do not spread. With two defects [Fig. 5(b)], two additional humps appear at the defect locations. Figure 6 shows a stable spreading droplet (with $\mathcal{N} = 50$, $\beta = 1.5$, and $h_0 = 1$) passing through a defect at $x_0 = 6$. The initial profile is shown in Fig. 6(a) and as the droplet spreads over the defect [Figs. 6(b)–6(d)], a single crest appears at its location. No surface instability is observed, consistent with LSA.

In all our simulations (see also Ref. [14]) defects do not appear to alter the stability of the bulk droplet. For a stable spreading droplet, a defect leads to a crest in the profile at large times, while for the unstable case, the defect gives rise to a pinned hump. Furthermore, in either case, defects do not influence spreading versus nonspreading behavior. They have only a local effect; global effects, such as surface anchoring strength over the whole droplet, are more likely to affect the spreading behavior.

In this work we have shown examples of stable spreading, unstable spreading, and unstable nonspreading droplets (as characterized in Ref. [6]), with and without defects. There are five parameters in our defect-free model ($\mathcal{C}$, $\mathcal{B}$, $\mathcal{N}$, β, and h_0) and it is in principle possible to modify stability by varying any of these. For simplicity, we varied only β and h_0, with other parameters fixed, and investigated the effect of defects on the evolution. We have examined other possibilities not shown here and have found similar qualitative behavior.

In conclusion, we presented an alternative model for spreading of a thin film of nematic liquid crystal that allows the free surface anchoring condition to relax as the film height goes to zero and can also account for the presence of defects. Simple linear stability analysis for a flat film appears to serve as a good indicator of the behavior of more complicated spreading drops. In particular, the presence of defects does not appear to alter the stability characteristics. While these 2D results are still some way from the quantitative simulations of the experimental results of Poulard and Cazabat [5], the 2D model presented here can exhibit the key experimental features of stable spreading, unstable spreading, and arrested instability. We believe our results provide valuable insight into the experimental observations and that our model is a good starting point for a full theoretical description of spreading nematic droplets.

This work was supported by the National Science Foundation under Grant No. DMS-0908158.

[1] D. W. Calton, K. Seunarine, G. Bodammer, and I. Underwood, IEE Proc. Optoelectron. **147**, 163 (2000).
[2] P. Palffy-Muhoray, Phys. Today **60**(9), 54 (2007).
[3] P. G. De Gennes and J. Prost, *The Physics of Liquid Crystals* (Oxford University Press, New York, 1995).
[4] S. Chandrasekhar, *Liquid Crystals*, 2nd ed. (Cambridge University Press, New York, 1993).
[5] C. Poulard and A. M. Cazabat, Langmuir **21**, 6270 (2005).
[6] L. J. Cummings, T.-S. Lin, and L. Kondic, Phys. Fluids **23**, 043102 (2011).
[7] F. M. Leslie, Adv. Liq. Cryst. **4**, 1 (1979).
[8] M. Ben Amar and L. J. Cummings, Phys. Fluids **13**, 1160 (2001).
[9] L. J. Cummings, Europ. J. Appl. Math. **15**, 651 (2004).
[10] C. Poulard, M. Voue, J. De Coninck, and A. M. Cazabat, Colloids Surf. A **282**, 240 (2006).
[11] N. Schopohl and T. J. Sluckin, Phys. Rev. Lett. **59**, 2582 (1987).
[12] R. B. Meyer, Mol. Cryst. Liq. Cryst. **16**, 355 (1972).
[13] R. V. Craster and O. K. Matar, Rev. Mod. Phys. **81**, 1131 (2009).
[14] See Supplemental Material at http://link.aps.org/supplemental/10.1103/PhysRevE.85.012702 for animations of some of the simulations.